Nonlinear Interactions of Two Incident Internal Waves

Tom E. Dobra[1], Andrew G. W. Lawrie[1] and Stuart B. Dalziel[2]

[1] Department of Mechanical Engineering, University of Bristol
[2] Department of Applied Mathematics and Theoretical Physics, University of Cambridge
tom.dobra@bristol.ac.uk

Abstract

We present experiments and analysis of the nonlinear interactions of two incident internal gravity wave beams of comparable amplitude. By using a wave maker consisting of a flexible boundary to a tank, driven by an array of independent actuators, incident beams of large amplitude several wavelengths in width are generated. Additional wave beams, produced via triadic interactions, are observed emanating from where incident beams of moderate amplitude cross. We decompose the fields, both temporally and spatially, in order to identify the transfer of energy between the modes. A perturbation approach is used to predict the the frequencies of the generated waves, which is in close agreement with observations. Finally, in the related configuration where the two incident frequencies are the same, wave breaking with the emission of other internal waves is observed when a large amplitude wave reflects off an interface.

1 Introduction

Internal waves in the ocean and atmosphere are generated by a variety of mechanisms, such as interaction with surface waves on the ocean produced by wind shear and flow over topography (lee waves). Due to their ubiquity in the oceans, it is inevitable that two such waves will intersect, which, if their amplitudes are sufficiently large, may lead to a nonlinear interaction. This is important for modelling the transport of energy within the oceans as well as for predicting where internal waves might break leading to the transfer of energy from larger scales to smaller scales (see e.g. Staquet and Sommeria (2002)).

Many of the well-known interactions depend on the conditions of triadic interaction,

$$\mathbf{k}_1 + \mathbf{k}_2 + \mathbf{k}_3 = 0, \tag{1}$$

$$\omega_1 + \omega_2 + \omega_3 = 0, \tag{2}$$

for three waves with wavevectors $\mathbf{k}_i$ and frequencies ω_i of either sign, to produce an energy exchange which occurs at second order. In the case of Boussinesq, linear internal waves, this can only occur if all three disturbances also satisfy the dispersion relation,

$$\omega = N \cos\Theta, \tag{3}$$

where Θ is the angle the wavevector makes with the horizontal and

$$N = \sqrt{-\frac{g}{\rho_0}\frac{d\rho_h}{dz}} \tag{4}$$

is the buoyancy frequency with reference density ρ_0 and background density stratification $\rho_h(z)$. In the well-studied case of parametric subharmonic instability in a linear stratification (uniform buoyancy frequency), only one wave is specified a priori, from which

a pair of waves is emitted, such that all three waves together satisfy the triads (1) and (2). Although several such pairs can exist for a given incident wave, the pair with the fastest growth rate is observed (Bourget et al. (2013)). However, in this paper, two out of the three nonlinearly interacting waves are specified in a linear stratification, so the interaction conditions (1), (2) and (3) cannot necessarily be satisfied. Nonetheless, the emission of additional waves by nonlinear interactions is still observed.

The structure of this paper is as follows. The experimental setup is described in section 2, before describing a common observed regime in section 3. In section 4, weakly nonlinear theory for the configuration is discussed and motivates further experiments in section 5. Finally, the conclusions are presented in section 6.

2 Experimental Setup

Two-dimensional internal wave fields were produced using a wave maker (shown in figure 1) in the form of a 1 m long flexible boundary to the base of a tank. It consists of a computer-controlled array of 100 horizontal rods actuated to move vertically with a neoprene foam sheet attached across them. This allows the boundary to take any non-overfolding shape, which can vary in time and include multiple frequencies simultaneously along all or part of the wave maker. Unlike recent cam-driven wave generators, first described by Gostiaux et al. (2007), no mechanical intervention is required to reconfigure the output between experimental runs. The neoprene sheet has a significant bending stiffness which acts to smooth the form of the boundary, resulting in clean, largely monochromatic wave fields. This is further improved by having beams many wavelengths across due to the large horizontal extent of the wave maker, minimising the edge effects of the wave maker. In addition, by preventing flow around the rods, much larger amplitude waves can be generated compared to those by oscillating bodies.

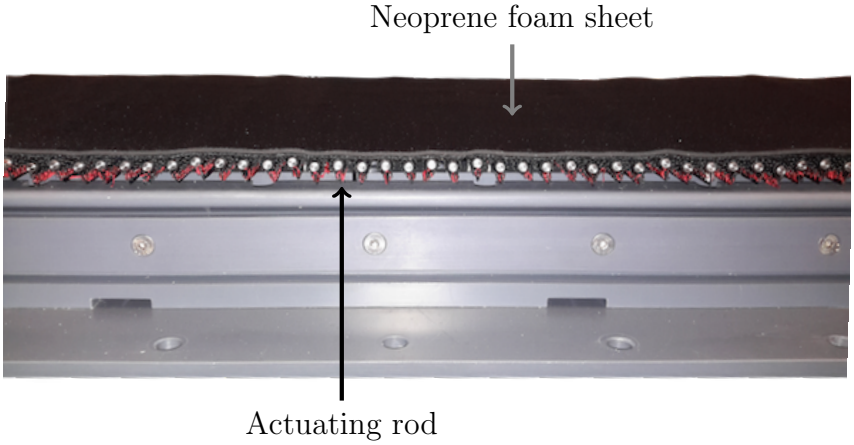

Figure 1: Wave maker viewed side-on. The tank walls (not present) are parallel to the page and flushed with the ends of the rods.

The tank containing the wave maker is 11.4 m long and 255 mm in width and was filled with a linear density stratification with an approximate buoyancy frequency N of 1.5 rad s^{-1} to a depth of around 300 mm. In the experiments, due to salt diffusion and evaporation of water from the top creating a mixed layer at the surface, the depth over

which the tank was stratified was typically 50 mm less than this. Because the generated flows are largely uniform across the tank, the technique of synthetic schlieren, as described by Dalziel et al. (2000), was used to obtain quantitative images of the wave fields: a camera placed in front of the tank films the distortions of a random black-and-white dot pattern placed behind the tank due to variations in the refractive index caused by variations in the density of the fluid; inverse ray tracing infers the density field within the tank.

3 Initial Experimental Results

The left side of the wave maker was driven with a right-travelling sinusoid at one frequency ω_1 with the one in the same direction on the right hand side at a different frequency ω_2. In both cases, the forcing was 150 mm across horizontally plus a 30 mm linear taper on each side, leaving a 640 mm stationary section between the waves. The amplitudes of the oscillations were increased linearly from rest in order to attain larger waves with only limited turbulence near the wave maker. A representative wave field is shown in figure 2 for $\omega_2 = 2.2\omega_1$: the first beam reflects off the interface at the top to then intersect the second beam within the grey box. A nonlinear interaction generates a third beam travelling diagonally up and to the right with amplitude constant in time, which shows that this is not an instability. Other nonlinearities are also present in the image, including the second harmonic from the left hand oscillations which undergoes a similar interaction with the main beam from the left side.

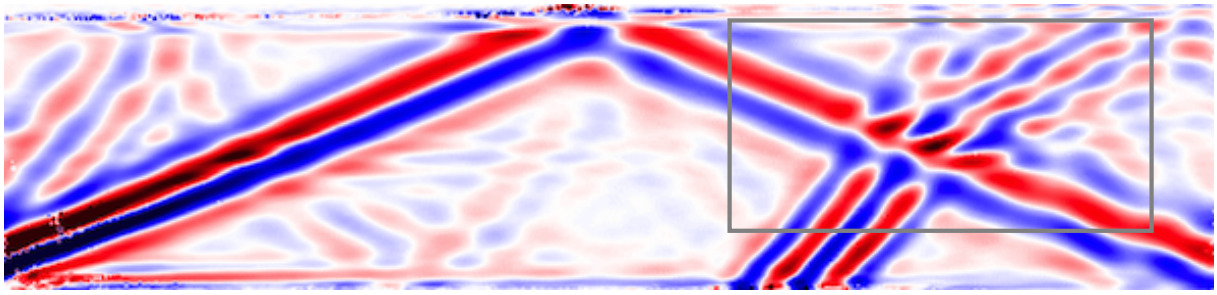

Figure 2: Wave field (vertical gradient of density perturbation) produced for $\omega_1 = 0.55\,\mathrm{rad\,s^{-1}} \approx 0.37N$ and $\omega_2 = 2.2\omega_1$ with vertical displacement amplitudes of 15 mm and 7.5 mm respectively and the same horizontal phase speed of $10\,\mathrm{mm\,s^{-1}}$.

The image in figure 2 is one frame in a video from which the frequencies of each of the oscillations can be extracted using dynamic mode decomposition (DMD), described in Schmid (2010). This technique does not require any knowledge of the underlying system, but assumes it can be approximated by some linear operator (here, not varying in time) from one frame to the next and finds an eigendecomposition of this operator with eigenvalues corresponding to the temporal frequencies and eigenvectors corresponding to the spatial mode shapes. Some of the modes for this case are shown in figure 3, with the three largest root-mean-square amplitudes corresponding to the first three images (in order). The modes in images 3a and 3b are those of the incident beams, while the third most significant (image 3c) contains the additional generated wave beam which it shows to have a frequency equal to the difference between the first two. Furthermore, it is clear that this third beam was not incident on the interaction zone from the bottom-left, and has gained most of its energy from beam 2 (frequency $2.2\omega_1$ from the right hand side). The next four modes are at frequencies corresponding to second harmonics

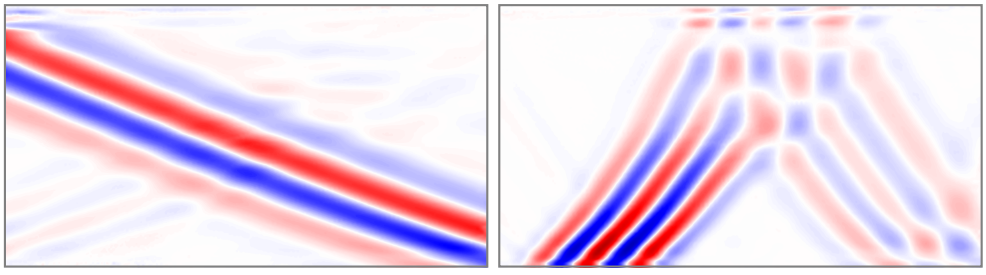

(a) $\omega = \omega_1 = 0.55\,\mathrm{rad\,s^{-1}}$ (b) $\omega = 2.2\omega_1 = 1.21\,\mathrm{rad\,s^{-1}}$

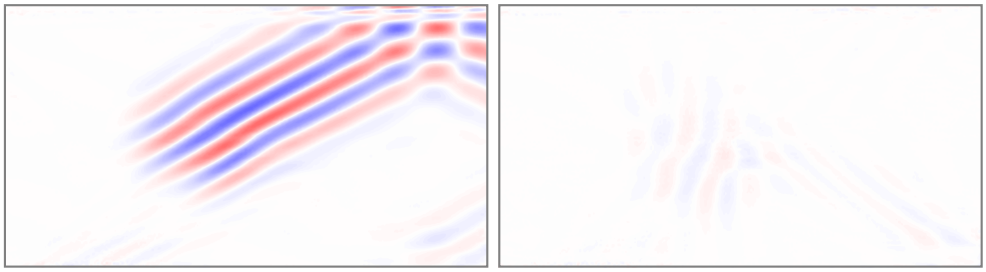

(c) $\omega = 1.2\omega_1 = 0.66\,\mathrm{rad\,s^{-1}}$ (d) $\omega = 3.2\omega_1 = 1.76\,\mathrm{rad\,s^{-1}}$

Figure 3: Real parts of four modes of dynamic mode decomposition of interaction between beams of frequency ω_1 and $2.2\omega_1$. All are at the same scale as and the window corresponds to the grey box in figure 2.

of the incident waves and their interactions, then figure 3d corresponds to the sum of the incident frequencies. This signal is almost invisible at the same scale and does not propagate outside the interaction zone primarily because its frequency is greater than the buoyancy frequency. In addition, by performing the Hilbert transform (filtering to retain only the Fourier modes with wavevectors in the quadrant of interest, which is useful because the wavevector has the same horizontal but opposite vertical direction to the group velocity for internal waves), it is observed that there is negligible backscatter from the interaction zone, i.e. all of the transmitted energy flux in the three beams is to the right (the same as the incident fluxes).

4 Weakly Nonlinear Theory

Linear theory states that any incident waves should pass through each other with no interaction, which is approximately true for small amplitudes. At larger amplitudes, a perturbation approach is used. The governing equations for an inviscid, linearly stratified fluid under the Boussinesq approximation are conservation of momentum (Navier-Stokes),

$$\rho_0 \left(\frac{\partial \mathbf{u}}{\partial t} + \mathbf{u} \cdot \nabla \mathbf{u} \right) = -\nabla p - \rho' g \mathbf{e}_z, \tag{5}$$

mass,

$$\frac{\partial \rho'}{\partial t} + w \frac{d\rho_h}{dz} + \mathbf{u} \cdot \nabla \rho' = 0, \tag{6}$$

and volume,

$$\nabla \cdot \mathbf{u} = 0, \tag{7}$$

where ρ_0 is the reference density, $\mathbf{u} = (u, w)$ is the velocity, t is time, $\mathbf{x} = (x, z)$ is the position, p is the pressure perturbation and ρ' is the density perturbation to the background density ρ_h. The quadratic nonlinear terms are $\mathbf{u} \cdot \nabla \mathbf{u}$ in (5) and $\mathbf{u} \cdot \nabla \rho'$ in (6),

which a linear model would assume to be negligible. In fact, these terms are indeed zero for a monochromatic wave of arbitrary amplitude, because the velocity $\mathbf{u}$ lies parallel to the lines of constant phase. In beam 1, let

$$\mathbf{u} = \mathbf{u}_1 = \frac{1}{2}\left(\hat{\mathbf{u}}_1 e^{i[\mathbf{k}_1\cdot\mathbf{x}-\omega_1 t]} + \text{c.c.}\right) \tag{8}$$

and similarly for ρ' and beam 2, where c.c. denotes the complex conjugate and the form has been selected to ensure the quantities are real. Since the beams have finite width, they in reality contain a spectrum of wavenumbers, all of which can interact to produce a new spectrum; however, monochromatic waves are considered here for simplicity. The quadratic terms in the interaction zone (where both incident waves are present) are of the form

$$Ae^{i[(\mathbf{k}_1+\mathbf{k}_2)\cdot\mathbf{x}-(\omega_1+\omega_2)t]} + Be^{i[(\mathbf{k}_1-\mathbf{k}_2)\cdot\mathbf{x}-(\omega_1-\omega_2)t]} + \text{c.c.} \tag{9}$$

for some constants A, B. In other words, the quadratic terms provide a small source term with wavevectors

$$\mathbf{k}_{3\pm} = \mathbf{k}_1 \pm \mathbf{k}_2 \tag{10}$$

and frequencies

$$\omega_{3\pm} = \omega_1 \pm \omega_2. \tag{11}$$

These are the triadic interaction conditions (1), (2) discussed in section 1, but in general $\mathbf{k}_{3\pm}$, $\omega_{3\pm}$ do not satisfy the dispersion relation (3). Instead, these force steady (non-growing) oscillations with such wavevector and frequency only in the interaction zone. These disturbances manifest themselves on the edge of the zone distorting the material surfaces in a manner similar to the wave maker, generating internal waves of frequency ω_3 which propagate away with a wavevector satisfying the dispersion relation. By necessity, the wavevector will undergo a spatial transition to achieve this, as can be seen in the wobble in figure 3c where the beam crosses the edge of beam 1 (figure 3a). Here, relatively little adjustment is required, leading to a strong transfer of energy to this third wave, but weaker interactions occur where this is less well-tuned. A particularly interesting case, which is yet to be tested, is when the forced oscillations do satisfy the dispersion relation; then one might expect persistent growth in amplitude of an internal wave - a condition of resonance.

5 Further Experimental Observations

5.1 Sum of Frequencies less than Buoyancy Frequency

Having two sets of forced oscillations presents two opportunities for generated waves: $\omega_3 = \omega_2 - \omega_1$ and $\omega_4 = \omega_2 + \omega_1$ provided $0 < |\omega_3|, |\omega_4| < N$. The wave with frequency ω_3 is present in figures 2 and 3, but ω_4 is absent because it is above the buoyancy frequency so produces an evanescent disturbance outside the interaction zone. However, if ω_2 is reduced such that $\omega_4 = 2.5\omega_1 \approx 0.92N < N$, a fourth wave of frequency ω_4 is emitted in addition to that with ω_3, as shown in figure 4. The fourth wave appears fairly weak because the vertical gradient of the density perturbation is shown but the gradient close to horizontal. A plot of the horizontal gradient only for this mode (obtained from DMD), shown in figure 5 at the same scale as figure 4, indeed confirms the presence of the mode and shows that the produced wave initially propagates diagonally up and to the right before reflecting off the top interface to produce the wave propagating down and to the right, as labeled in figure 4.

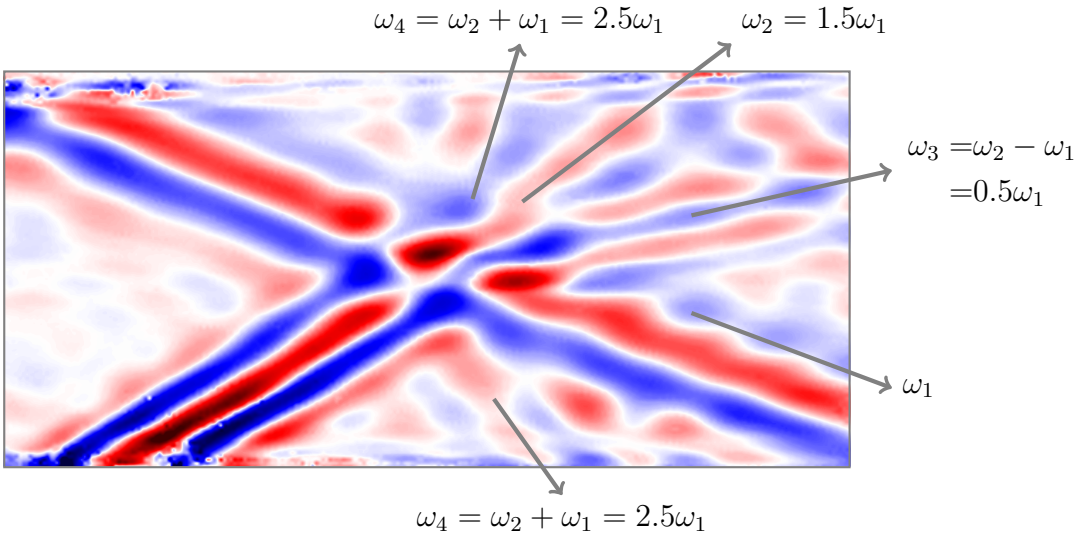

Figure 4: Vertical gradient of density perturbation for $\omega_1 = 0.55\,\mathrm{rad\,s^{-1}} \approx 0.37N$ and $\omega_2 = 1.5\omega_1$ with vertical displacement amplitudes of 15 mm and 7.5 mm respectively and the same horizontal phase speed of $10\,\mathrm{mm\,s^{-1}}$.

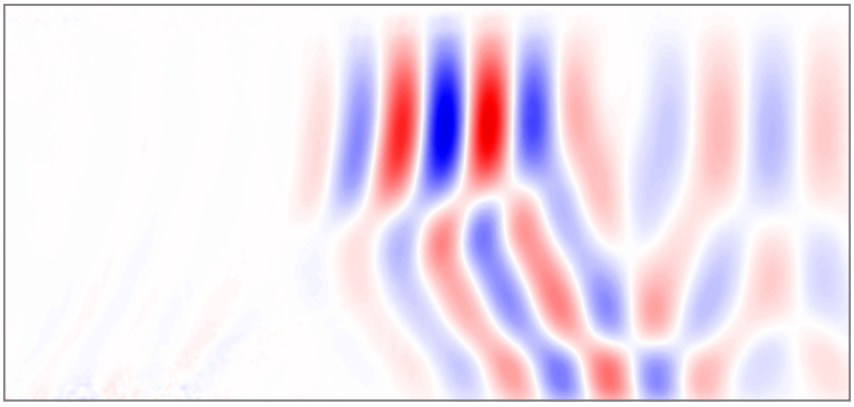

Figure 5: Horizontal gradient of density perturbation of mode $\omega_4 = \omega_1 + \omega_2$ for $\omega_1 = 0.55\,\mathrm{rad\,s^{-1}} \approx 0.37N$ and $\omega_2 = 1.5\omega_1$.

5.2 Wave Breaking on Reflection

As a third configuration, shown in figure 6, the second incident wave was driven at double the frequency of the first ($\omega_1 = 0.65\,\mathrm{rad\,s^{-1}} \approx 0.43N$, $\omega_2 = 2\omega_1$), but with the same horizontal wavenumber $k_1 = k_2 = 0.065\,\mathrm{rad\,mm^{-1}}$. This time, only a weak triadic interaction occurred where the beams crossed, because the theoretical horizontal wavenumber of the forced oscillations is zero, resulting in little attenuation of the second incident beam prior to reaching the interface at the top of the tank. As predicted by linear theory, the wave reflected off the interface to proceed down and to the right. Near the interface, one might expect a triadic interaction between the incident and reflected waves, but this is not possible since $\omega_3 = 0$ and $\omega_4 > N$. Furthermore, because of the large amplitude of these incident and reflected waves combined at the same location, a wave breaking event occurred just below the interface. Patches of apparently saturated signal within the interaction region are attributed to turbulence locally destroying the coherence of the optical signal used in calculating density perturbations. Moreover, a new wave beam was emitted down and to the left from this region.

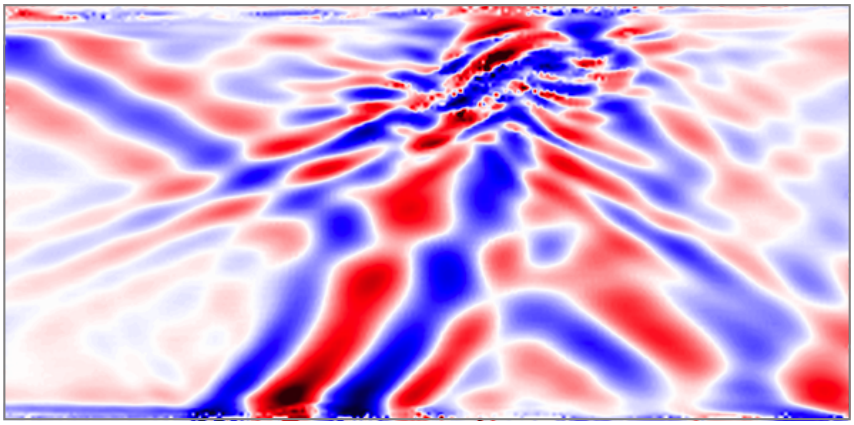

Figure 6: Vertical gradient of density perturbation for $\omega_1 = 0.65\,\mathrm{rad\,s^{-1}} \approx 0.44N$ and $\omega_2 = 2.0\omega_1$ with vertical amplitude of 7 mm. Wave breaking occurs in the top-centre of the image.

The four most significant modes of the dynamic mode decomposition are shown in figure 7. Figure 7a shows the usual third wave is still present, albeit weaker, while the strong zero mode in figure 7c is indicative of mass displaced by the wave breaking. Because of the strong nonlinearities in the flow, the linear operator approximation used in DMD was unable to completely resolve the modes, causing notable leakage between the modes. Nonetheless, figure 7d provides a reasonable estimate of $0.51\,\mathrm{rad\,s^{-1}}$ for the frequency of the generated wave propagating down and to the left, which is confirmed by considering its angle to the vertical and the dispersion relation (3). By using the Hilbert transform, it can be seen that this wave originates in the breaking zone with waves departing in all four directions, like a St. Andrew's Cross for an oscillating body. Also, the next mode in the decomposition has frequency $0.76 \approx 1.3 - 0.51\,\mathrm{rad\,s^{-1}}$ suggesting another triadic interaction. Since these frequencies are not directly excited by the wave maker, and that all the disturbances were growing substantially faster than the rate at which the amplitude of the forcing was increasing, this suggests further instabilities just below the interface in addition to those discussed here.

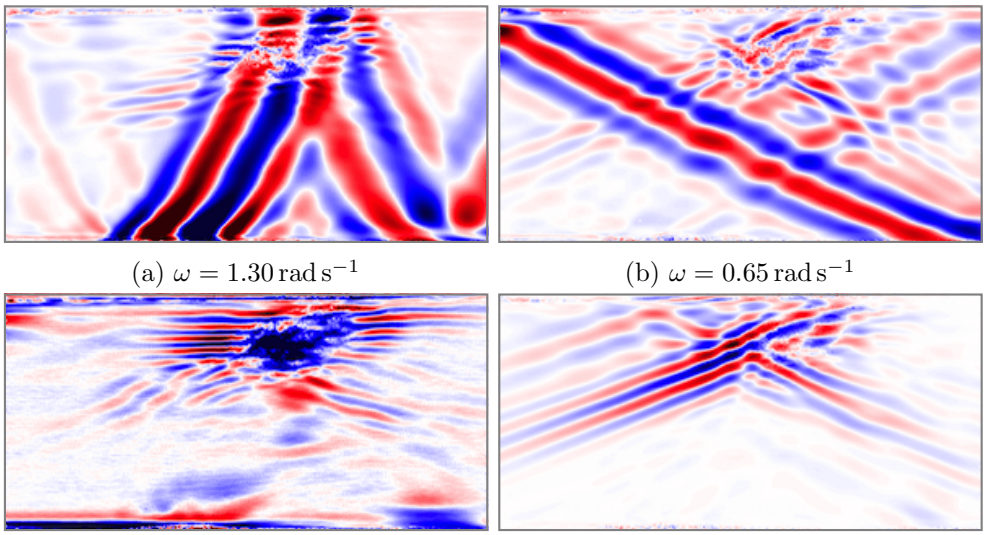

(a) $\omega = 1.30\,\mathrm{rad\,s^{-1}}$ (b) $\omega = 0.65\,\mathrm{rad\,s^{-1}}$

(c) $\omega = 0.00\,\mathrm{rad\,s^{-1}}$ (d) $\omega = 0.51\,\mathrm{rad\,s^{-1}}$

Figure 7: Most significant modes of dynamic mode decomposition of figure 6, ordered by root-mean-square amplitude.

6 Conclusions

Two distinct nonlinear regimes have been observed for the intersection of two internal waves. First of all, two moderately large-amplitude incident waves can drive two sets of forced oscillations within a confined region, one with wavevector and frequency equal to the difference between those of the incident waves, the other at the difference. If the parameters are sufficiently well-tuned and the frequencies of the generated oscillations lie below the buoyancy frequency, then this region emits strong internal waves with the generated frequency and a wavevector adjusted to be consistent with the dispersion relation. This behaviour occurs for a broad range of parameters and appears to be stable, although is theoretically unstable if the forced oscillations satisfy the dispersion relation for internal waves - a resonant interaction condition. Secondly, if the two incident waves have the same frequency which is greater than half the buoyancy frequency, as occurs near a reflective boundary, the waves may break, leading not only to a patch of turbulence, but the emission of other internal waves at frequencies which are not directly related to the input frequency.

References

Bourget, B., Dauxois, T., Joubaud, S., and Odier, P. (2013). Experimental study of parametric subharmonic instability for internal plane waves. *J. Fluid Mech.*, 723:1–20.

Dalziel, S. B., Hughes, G. O., and Sutherland, B. R. (2000). Whole-field density measurements by 'synthetic schlieren'. *Exp. Fluids*, 28:322–335.

Gostiaux, L., Didelle, H., Mercier, S., and Dauxois, T. (2007). A novel internal waves generator. *Exp. Fluids*, 42:123–130.

Schmid, P. J. (2010). Dynamic mode decomposition of numerical and experimental data. *J. Fluid Mech.*, 656:5–28.

Staquet, C. and Sommeria, J. (2002). Internal Gravity Waves: From Instabilities to Turbulence. *Annu. Rev. Fluid Mech.*, 34:559–593.